Département Sciences de la matière
École Normale Supérieure de Lyon
Université Claude Bernard Lyon I

Yohann Faure
July 14, 2021
M2 Complex Systems

The Onset of Sliding of a **Granular Frictional Interface**

Abstract:

Frictional interfaces are a major part of both geophysics and engineering, be it in the study of friction in machines or that of friction between tectonic plates. The historical models based on Coulomb's Law to describe friction between two coarse surfaces with microscopic asperities have been extensively studied, describing any frictional movement as either sticking or slipping, but the transition from the stick phase to the slip phase remains a recent field of study from the experimental point of view. This transition has direct application in seismic hazard prevention and industrial design, and fundamental implications in materials physics.

This internship extends some of the fracture mechanics results obtained in the case of a coarse interface between two elastic blocks to the case of the rupture of a frictional interface composed of a thin layer of granular media compressed between two elastic blocks. This perturbative approach using only a thin layer of grains is an original work and is to be continued during a three-year PhD.

The main results of this internship are the design and construction of an adaptive experimental setup allowing for the simultaneous observation and characterization of rupture fronts and normal and shear forces applied to the blocks, as well as a set of preliminary results on granular interface friction and crack propagation in granular media.

Keywords:

Granular Material, Seismology, Frictional Interface, Rheology, Experimental Physics.

This internship was supervised by **Elsa Bayart**, CNRS researcher, ENS de Lyon.

Acknowledgements

This internship was made possible by several people that I would like to thank.

I want to express my deepest appreciation to my advisor Elsa's helpful advice and relentless support through all of my internship, as well as for the valuable knowledge she passed on to me. I look forward to our future collaboration during my PhD.

I would like to extend my sincere thanks to all the PhD students of the lab, and especially the 1145 team. I wish you all the best, let's keep that vibe grooving!

Thanks also to all the lab staff, all the professors and researchers, who have provided me with help, advice, equipment, and sometimes cake during the coffee break. You are a fantastic team to work with, and make up the best work atmosphere I've encountered in a laboratory yet.

As this internship concludes my time as a Normalien, I would like to give special thanks to the dearest friends I made here in Lyon, non-exhaustively and in a Python-generated pseudo-random order, Diane, Louis, Aurélien, Youssef, Nicolas, Rémi, Aurélia, Aubin, Louis, Élodie, Garance, Thomas, Ruben, Solène, Nicolas, William, Paul, Nacim, Matthieu, Henry, Flora, Joël, Antonin, Marlysa, and to the school Brass Band, La Fanfarovis.

I finally gratefully acknowledge the effort of the internships evaluation committee, that of Pierre Borgnat and all the teaching team of the Physics and Complex Systems Masters, as well as Guillaume Laibe's commitment and help as my tutor throughout the past four years at the ENS de Lyon.

Thanks to all!

Contents

1 Introduction

Frictional interfaces are at the core of many fundamental and applied research fields, from the large scales of geophysics to nanotribology, yet its understanding is far from perfect in many aspects. When considering dry interfaces, the friction force stems from a complex combination of electrostatic adhesion, surface roughness, and elastic or plastic deformation, making any attempt of direct computation from the first principles of mechanics impractical.

As a means to elude that complexity, the first empirical laws describing friction emerged during the Renaissance era, under the impulsion of Leonardo Da Vinci, followed by Amontons during the 17th century, and Coulomb during the 18th. These laws however did not reflect the local complexity of the interface, but rather described a macroscopic behavior, oblivious to the microscopic mechanisms at play.

One of the main questions that these models do not elucidate is that of the transition from a static contact to a dynamic contact between two solids during a stick-slip motion [1]. This transition is of utmost importance in Geophysics, as stick-slip is considered to be one of the mechanisms at play during earthquake [2, 3]. These dynamics have been extensively studied for coarse interfaces [4, 3], coarse meaning that the contact surface has asperities larger than the atomic scale, revealing the existence of crack-like dynamics during the transition from static to dynamic contact. For a granular interface, this transition has been extensively studied in the framework of rate-and-state models [5], but the field remains open for the interfactial rupture mechanisms study.

An interface is considered granular when the contact area between two frictional solids is not unibody, but rather composed of small solid grains, namely a gouge layer or a third body. A seismic fault would be a case in point as such faults lead to a grinding mechanism that crushes the interfacial rocks to gravel-like or sand-like grains. Systems with a granular interface are more complex than a coarse interface, as the dynamics can be heavily influenced by the nature of both the bulk of the solids and the grains between them.

During my Master's research internship, supervised by Elsa Bayart at the Laboratoire de Physique of the ENS de Lyon, I studied an ideal case of granular interface, using blocks of PMMA and a thin layer of 2D Nylon grains under external shear stress. This study revealed the existence of a crack-like behavior in granular interfaces, similar to the coarse interface, and aimed at characterizing it as extensively as possible. This work is inscribed in a broader perspective, as I will be continuing my research on the subject during my PhD, under the supervision of Elsa Bayart.

This report briefly presents the standard theory of fracture applied to coarse frictional interfaces and its experimental verification. It then goes into more detail about the experimental setup and the different measurements we designed. Finally, it describes the experiments we conducted to characterize the granular interface, the various results we obtained, and a discussion about their implications for further developments.

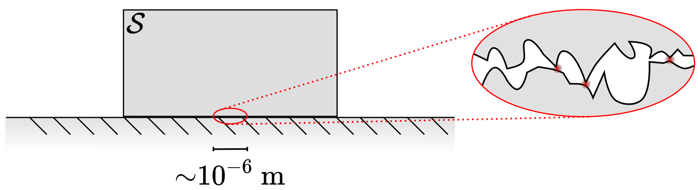

Figure 1: Schematic representation of the real contact area between two solids, at the microscopic scale. The red blurred dots represent the points bearing the normal force.

2 Friction theory for a coarse interface

In this section, we will first detail the historical approach to friction, namely Coulomb's Law, in a stick-slip motion case. We will then focus on the phenomenology of the transition between the stick phase and the slip phase, *i.e.* the detachment of the contacting surfaces, and its modeling in the framework of the theory of fracture. The end of the section will consist of a discussion of the main differences between a rough interface and a granular interface.

2.1 Coulomb's Laws

Friction appears between two objects when they are put into contact and an operator tries to make one of them slide onto the other. It is a force that goes against such movement, holding the two solids together. This force stems from the asperities of the solids interlacing on the surfaces (Fig. 1). This roughness, appearing from the nanometer scale to the millimeter scale depending on the solids, causes the material to resist sliding in the case of a rough interface. Literature about atomically smooth interfaces does exist [6, 7], but is out of bounds for this internship.

This asperities entanglement makes the elaboration of a conceptual theory of friction very hard, as it would depend highly on the material considered. Therefore, physicists have developed a set of empirical laws, known as Coulomb Laws of Friction, that first relied on observations, and were theoretically explained later on. These laws, established by Charles-Augustin de Coulomb [8], state that when applying a shear force or traction force F_t on a solid body that has previously been loaded by a normal force F_n, a third force F_f known as *force of friction* appears in opposition to the movement. This force, exerted by each surface on the other, is parallel to the contact surface, opposite to F_t (Fig. 2).

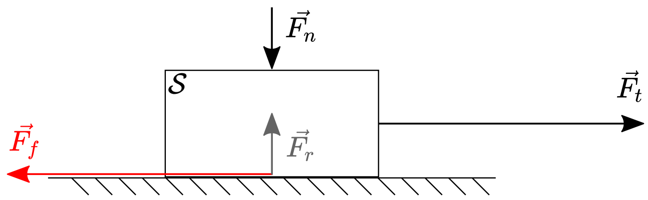

Figure 2: Schematic representation of the forces applied on solid $\mathcal{S}$, as described by the Coulomb Law, including the normal reaction F_r.

These laws state that there exists a certain *static friction coefficient* named μ_s such that as long as $\|F_t\| \leq \mu_s \|F_n\|$, no sliding occurs, it is the *stick phase*. Conversely, as soon as $\|F_t\| = \mu_s \|F_n\|$, the solid starts sliding, it is the *slip phase*. In this phase, the friction coefficient changes to a new *dynamic friction coefficient* named μ_d such that as long as the two solids slide one onto the other, $\|F_f\| = \mu_d \|F_n\|$.

A conceptual justification for these laws emerged in the middle of the 20$^{\text{th}}$ century [9]. This explanation conceptualizes the fact that the real contact area A_r is much smaller than the apparent one, because of all the microcontacts at play. Hence, when increasing F_n, those microcontacts easily reach the yield stress σ_Y of the material, *i.e.* its plastic limit. At that point, increasing F_n amounts to an increase of A_r, following the $F_n = \sigma_Y \times A_r$ law. To trigger a slip event, the shear stress then has to reach τ_S the shear strength of the contact, such that $F_f = \tau_S \times A_r$. At that point, $F_f = \frac{\tau_S}{\sigma_Y} \mathrm{F}_n = \mu_s F_n$, and all contacts break at the same time.

This approach is however proved wrong because it considers that the stresses are uniform along the interface and that all the interface starts slipping simultaneously. Furthermore, μ_s has long been thought to be a material characteristic, but its value can vary from sample to sample, and depends on many factors such as lubrication, rugosity, temperature, and the history of the interface [10].

2.2 Minimal stick-slip motion example

Coulomb's law leads to the prediction of stick-slip motion, that to a certain extent can accurately describe the movement of many macroscopic systems, from sliding trolleys to rudimentary seismic faults [2]. Stick-slip motion occurs when normally loading an interface between two solids with some form of elasticity, and applying a shear force. It consists of a succession of stick phases, during which the two solids have no relative movement, and slip phases, during which the two solids slip one on another (Fig. 3).

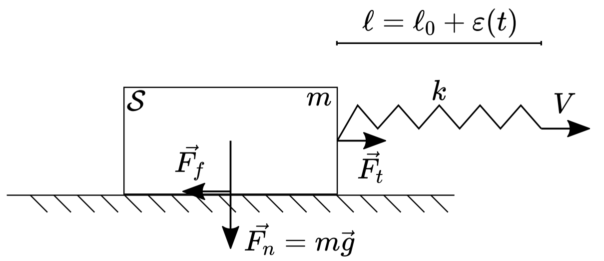

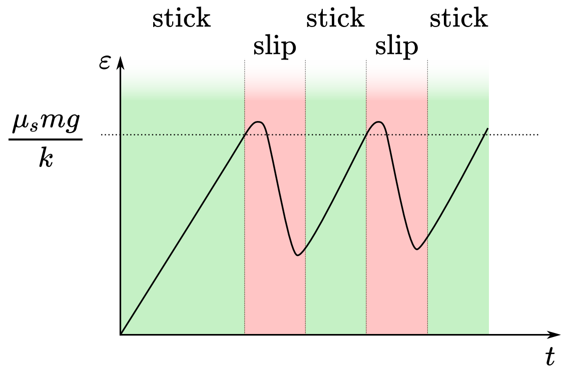

Figure 3: The typical stick-slip setup. **Left:** Standard experimental setup used to obtain macroscopic stick-slip motion. The solid $\mathcal{S}$ under the gravity of its mass m is tied to the end of a spring of constant k, which second end is moving at constant velocity V. The length of the spring is named ℓ, with ℓ_0 its free length. **Right:** Standard evolution of $\varepsilon(t)$, elongation of the spring, when starting with a non-moving solid $\mathcal{S}$. The motion observed consists of stick and slip phases, alternating regularly.

At $t = 0$, the solid $\mathcal{S}$ is static, and the spring starts free ($\varepsilon = 0$) and gets longer with a constant speed V. Applying Newton's and Coulomb's Laws, $\mathcal{S}$ cannot move while $F_t = k\varepsilon < F_f = \mu_s mg$. That means the solid sticks until $t_1 = \mu_s mg/Vk$. But as soon as this limit is reached, movement occurs, and the value of F_f changes to $F_f = \mu_d mg$. Therefore, if $\mu_s > \mu_d$, the solid keeps slipping. A new application of Newton's Law gives Equation 1, with x the position of $\mathcal{S}$, then solved in Equation 2.

$$m\ddot{x} = k\varepsilon - \mu_d mg \iff \ddot{\varepsilon} + \omega_0^2\varepsilon = \mu_d g \qquad \text{with} \qquad \omega_0 = \sqrt{\frac{k}{m}} \tag{1}$$

$$\varepsilon(t > t_1) = L\cos(\omega_0(t - t_1) + \phi) + \frac{f_d mg}{K} \qquad \text{with} \qquad \begin{cases} L^2 = \left(\frac{(\mu_s - \mu_d)mg}{k}\right)^2 + \left(\frac{V}{\omega_0}\right)^2 \\ \text{and} \\ \quad \phi = -\arctan\left(\frac{Vk}{(\mu_s - \mu_d)mg\omega_0}\right) \end{cases} \tag{2}$$

This solution stops applying whenever $\dot{x} = 0$, *i.e.* $\dot{\varepsilon} = V$, corresponding to a new stick phase, and the cycle repeats.

This minimal stick-slip model is accurate when describing macroscopic movement over a large enough area, such that no significant variation is made in the averaged contact properties. More accurate empirical modelings known as *rate and state laws* do exist [11] and describe in more detail the large-scale dynamics of a frictional interface, incorporating the time and velocity dependence of the real contact area and therefore of the friction coefficient. Yet these models do not explain the microscopic mechanism of the transition between the static and dynamic regime.

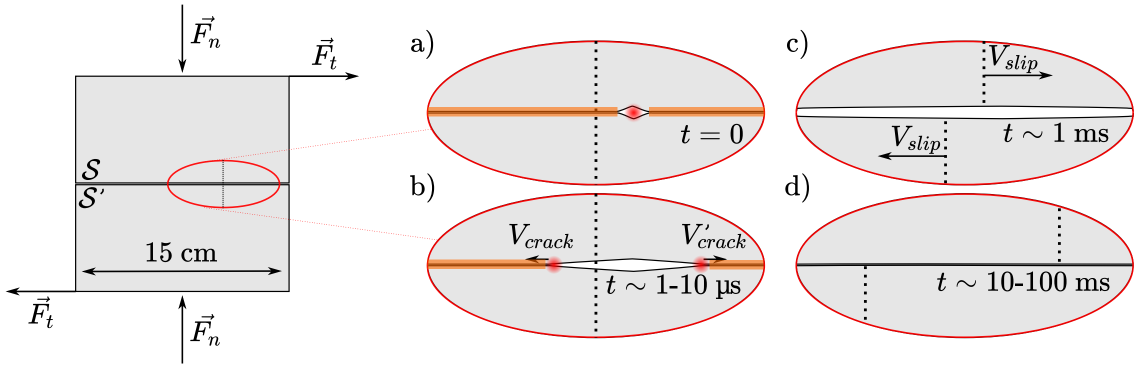

Figure 4: Schematization of the nucleation and propagation behavior of a crack, allowing the transition from a stick phase to a slip phase. The typical propagation speed is of the order of the speed of sound in the blocks [12]. The four steps go as follows: **(a)** Nucleation, **(b)** Propagation of the rupture front, **(c)** Slip phase, **(d)** Bounding the interface again. The orange line symbolizes the area under shear load, the red dot the disbound point in the interface, and the dotted line shows the global movement of the blocks.

2.3 From friction to crack propagation

This transition from stick to slip has been in the focus of research for years [12, 13, 14] in the case of a rough interface in direct contact. The observed behavior is that of a first local disbound most likely around an imperfection or a loading defect of the interface, called the *nucleation*, followed by the propagation of this disbound at speeds comparable to that of sound in the blocks. For finite-size systems, the macroscopic sliding movement then only starts when this propagating crack has reached both ends of the interface. These steps are described in detail in Figure 4.

This phenomenology, describing small time and spatial scale, contrary to Coulomb's description of friction, which is focused on macroscopic movements, has been documented and observed [15]. The main difference lies in the fact that Coulomb's model makes the disbound of the interface instantaneous, while the observation shows the propagation of a disbound front. That front propagates like a fracture at the interface, and this aspect is a core consideration in this field.

2.4 Modeling and theory of fracture

Despite the difference between the two systems, the dynamics and strain fields of frictional ruptures can be accurately described by the theory of brittle fracture, Linear Elastic Fracture Mechanics (LEFM), with the supposition that the interface is a preferential plane for the propagation of a crack [15].

Brittle fracture occurs when breaking a single block under stress. When such a block breaks, a rupture propagates from one end to the other, leading to the shattering of the block. This rupture is called a *crack*. Conceptually, a crack is a stress-free line (surface) inside a 2D (3D) solid. These cracks can be sorted in three *modes* according to the direction of loading relatively to their direction of propagation (Fig. 5).

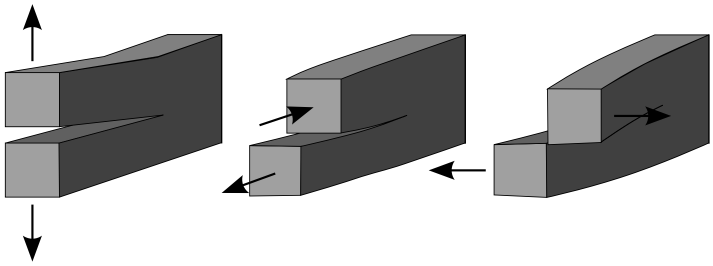

Figure 5: The three different crack modes. They are linearly independent and their contributions can be summed.

When limiting this discussion to sub-Rayleigh ruptures, *i.e.* ruptures that propagate at a lower speed than the Rayleigh wave speed of the material[1], we can consider the equations of linear elasticity. Close to the crack tip, for a solid with no stress along the crack line, and imposing the convergence of elastic energy, we find [16]:

$$\sigma_{ij} = \sum_{\alpha=\mathrm{I,II,III}} \frac{K_\alpha}{\sqrt{2\pi r}} \Sigma_{ij}^{\alpha} \left(\theta, C_{\mathrm{f}}\right) \tag{3}$$

In this equation, K_α is the stress intensity factor for each loading mode. It relates to the fracture energy of the material and contains information about the loading configuration and the geometry of the system. (r, θ) are the polar coordinates relative to the tip of the crack, as shown in Figure 6, and C_f is the instantaneous speed of the crack tip. The Σ_{ij}^{α} functions are known universal functions [16]. This square-root singularity of the elastic fields, which essentially defines brittle fracture, is universal in the sense that its form does not depend on the geometry and outer boundary conditions, and is regularized in the process zone (Fig. 6).

Although a mode II crack is unstable in brittle fracture, in the frictional crack setup, the weak frictional interface makes it able to propagate. Adding this information, we get Equation 4.

$$\sigma_{ij} = \frac{K_{\mathrm{II}}}{\sqrt{2\pi r}} \Sigma_{ij}^{\mathrm{II}} \left(\theta, C_{\mathrm{f}}\right) \tag{4}$$

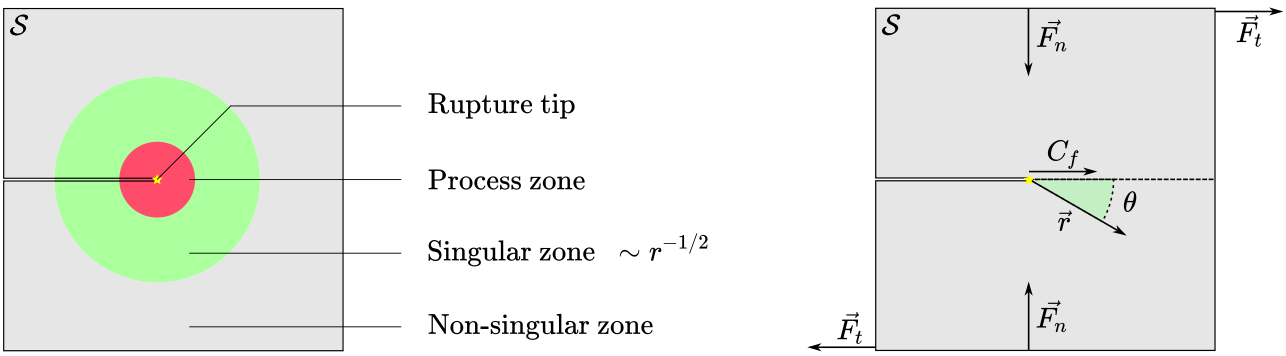

Figure 6: The process zone and the singular zone. **Left:** The zone in which Equation 3 holds is the singular zone, in green. The process zone, in red, corresponds to a physical regularization of the constraints. **Right:** The notations used in Section 2.4, with θ the angle relatively to the line of propagation of the crack, r the distance to the tip of the crack, and C_f the speed of the crack.

[1]Faster ruptures do exist, and are called supershear ruptures. Their propagation mechanism is different, and their speed limited by the speed of P-waves in the blocks.

When the crack propagates, $K_{\mathrm{II}} = \sqrt{\Gamma E / A(C_f)}$ with the Young Modulus E, the required energy to propagate the crack over a unit of surface, or *energy of fracture* Γ, and $A(v)$ a known function of the crack velocity C_f. The value of Γ can hardly be inferred theoretically. It depends on F_n and A_r. It reflects the dissipation properties of the crack tip opening. In the coarse PMMA interface case, we consider its value to be $\Gamma \sim 1\,\mathrm{J\,m^{-2}}$ [15].

Assuming the plane stress limit conditions for a 2D solid, from Equation 4 we can compute the displacement associated with the crack for each point (r, θ) of the material by using Hooke's law, the constitutive equation of an elastic material, that relates stress and deformation. When doing so, we obtain the results shown in Figure 7. From those results, we can define a typical order of displacement $\delta_{LEFM} = 1\,\mu\mathrm{m}$. This typical displacement corresponds to the minimum resolution necessary to see the propagation of the crack at the scale of the interface.

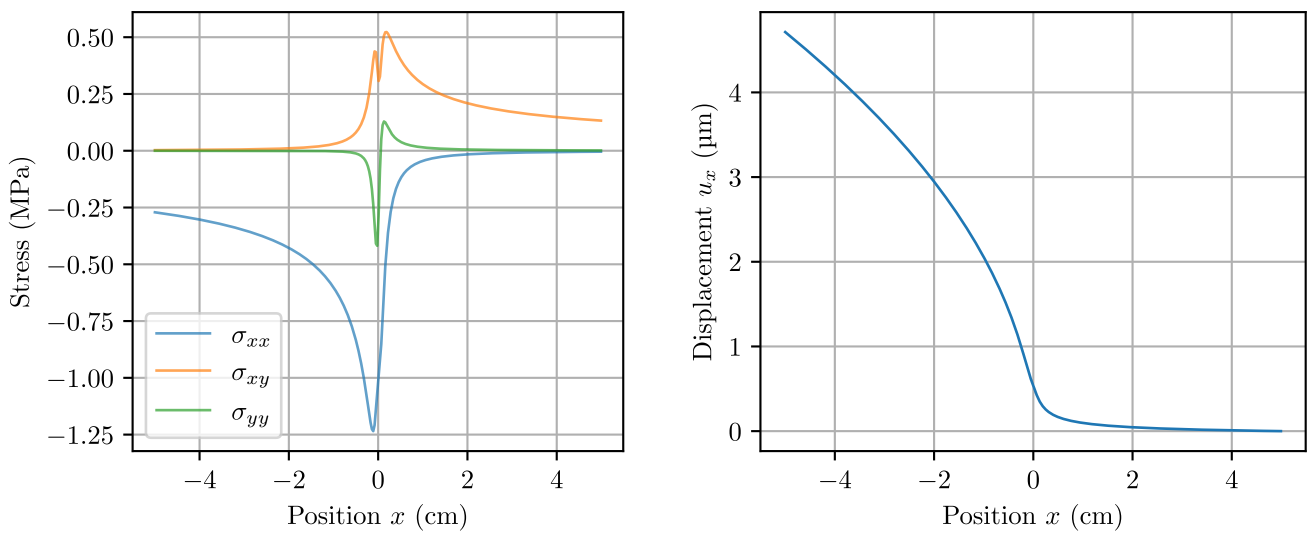

Figure 7: The LEFM solution for crack propagation. The position $x = 0$ corresponds to the position of the crack tip, propagating from left to right. We took $y = 1\,\mathrm{mm}$ above the interface, $\Gamma = 1\,\mathrm{J\,m^{-2}}$, and $C_f = 300\,\mathrm{m\,s^{-1}}$. **Left:** The three stress curves corresponding to the situation. **Right:** The corresponding displacement curve.

2.5 Position of the problem

The above results apply to a coarse interface. We are interested in the rupture mechanics of a granular fault. When considering a seismic fault, the nucleation and propagation of a disbound front are observed [17], similarly to what we observe for a coarse interface. Despite that phenomenology proximity, a fault has more layers of complexity, as in general, a seismic fault has a layer of crushed rocks trapped between the two blocks. This gouge layer is a granular material under pressure. The propagative rupture exists but has not been experimentally characterized, except for some qualitative attempts [18, 19]. To model this complex mechanical system, we chose to insert granularity as a perturbation of the coarse interface, expecting to trigger ruptures. In the case of a granular interface, we had to answer the following questions: does nucleation-propagation dynamics for a disbound front exist? Is the crack dynamics controlled by the elasticity of the grains or by that of the bulk? What is the influence of the properties of the granular material?

Please note that this problem is not a matter of granular materials rheology. In such rheology problems, the bulk of the solid applying shear stress is inelastic, and the granular material has to be thick. In our case, the interface is loaded by the elastic bulk of the material, and the thin granular material layer is of a similar elasticity as the bulk. This elastic bulk approach is the originality of this setup. *This is NOT a granular materials rheology problem.*

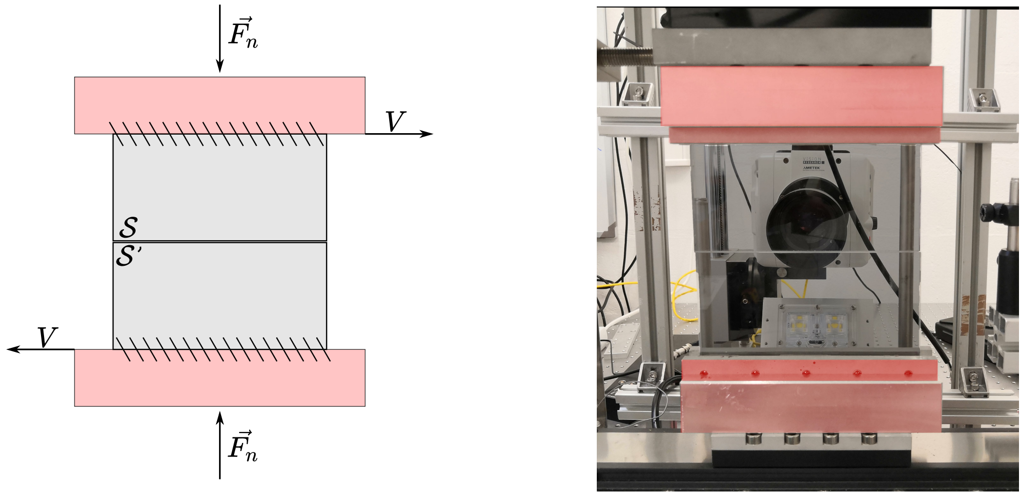

Figure 8: Schematic view and picture of the experimental setup used to study crack propagation. The normal force is applied through a press, and constant translation speed is applied to the block through a motor and a pair of inelastic jaw clamps.

3 Experiment design

3.1 Experiment principle

The global experimental setup, described in Figure 8, consists in pressing two blocks together under a normal force F_n, and shearing the system by imposing a tangential displacement at the bottom of the blocks. A granular medium is inserted at the interface between the two blocks. We aim at tracking the displacement of the grains at the onset of sliding of the frictional system, in order to detect propagating ruptures withing the granular layer.

To achieve this measurement, we have to consider a model system with a 2D granular layer, contrary to the classical 3D system. Such a 2D layer consists in a pile of cylinders of length the width of the blocks. In this configuration, each cylinder can be tracked using a high-speed camera and a particle-tracking algorithm.

3.2 Experimental setup

The first criteria on the block is that they must not buckle. According to Euler's critical load formula, the maximum force sustainable by a block is $F_{max} = \pi^2 EI/(KL)^2$, with I the second moment of area of the blocks, L their height, $E = 2.9\,\mathrm{GPa}$ their Young's modulus, and $K = 1$ a geometric coefficient due to the pinning of one end of the block. Using block of Poly(methyl methacrylate) (PMMA) 1 cm wide gives $F_{max} \simeq 2 \times 10^5\,\mathrm{kg}$. Therefore, 1 cm of PMMA is both sufficient and easy enough to produce. The transparency of PMMA is also a nice feature when considering certain types of measures.

The frame and motors, schematized and shown in Figure 9, have to hold the normal and shear loads. The model we used was a Zaber X-LRT linear stage. The main constraint for the motor was the precision of its command. After calibration using a high precision STIL-DUO interferometric position detector, the worm drive microsteps defined by the constructor (0.12 µm) was reliable enough for our use-case. A small scale (a few microsteps) hysteretic effect was noted, but as the loading of the interface takes a movement several orders of magnitude higher (∼10 µm), it is of little impact on the measures.

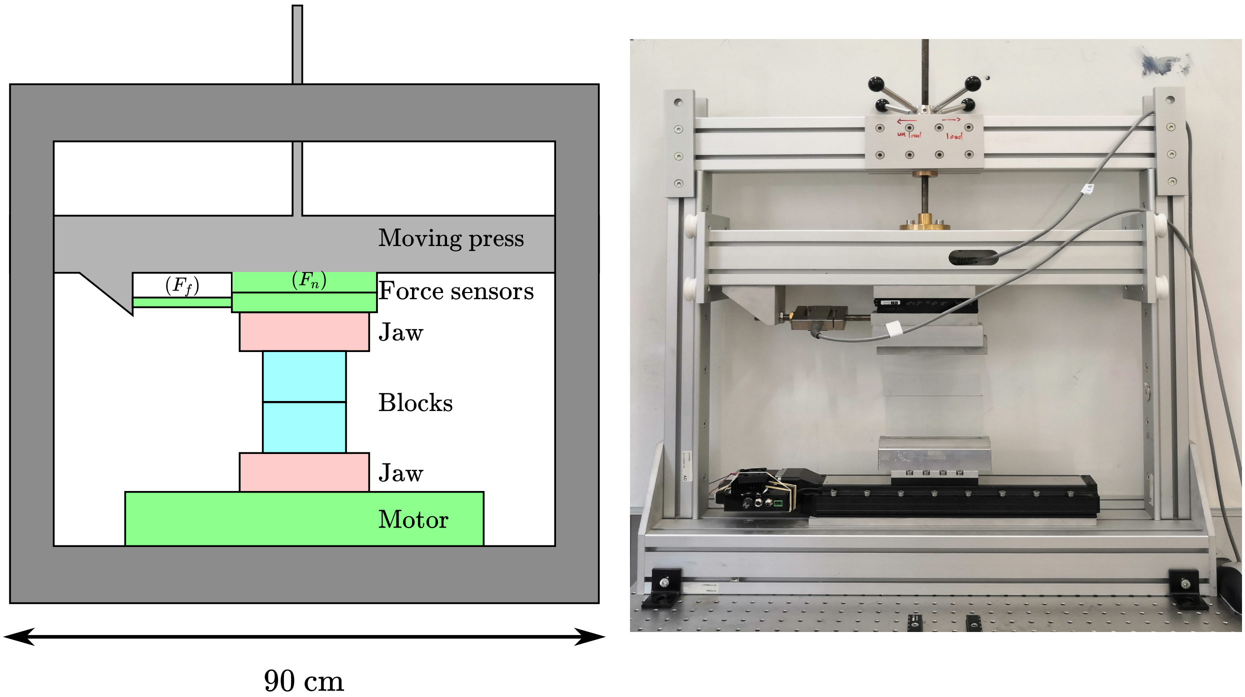

Figure 9: Schematization and picture of the frame used for the experiment. The press bar is screwed manually to increase or decrease the normal force F_n. Two captor in the press measure F_n and F_f.

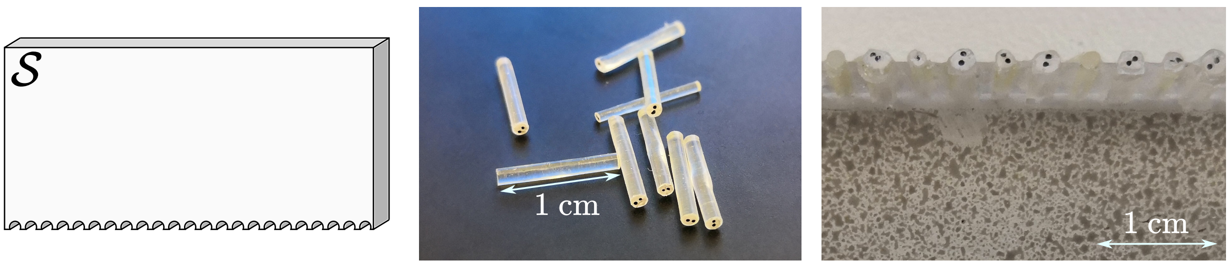

Figure 10: The different patterns used for the various optical measurements. **Left:** The granular blocks are regularly drilled along the interface. The grains are of two different calibers, 1.3 mm and 0.9 mm wide. **Middle:** The pattern used on the grains to detect their position. **Right:** The random pattern used to measure the deformations of the bulk of the blocks and to measure speed propagation with photodiodes.

The cylinders used to make the granular material are thick nylon strings (0.9 mm and 1.3 mm of diameter) straightened and cut to the appropriate length (1 cm). They are compressed between the two blocks of PMMA. To tightly bind them to the bulk of the blocks and ensure that sliding occurs in the granular media, we had to engineer specific blocks (Fig. 10). To avoid crystallization, we used two different diameters of grains. The size of the grains could be of major impact on the experiment, and its study is part of prospects, as well as the choice of material. We used 2 to 5 layers of grains, without counting the ones glued to the bulk. The influence of this thickness is out-of-bounds for this report but will be discussed in future works[2].

To ensure the transmission of shear force between the blocks and the granular media, we used specially engineered blocks. The first blocks used had a regular pattern, alternating large and small glued grains, to avoid crystallization inside the granular layer. The second prototype has a non-regular pattern, with positions of the drill holes randomly generated. Images of these prototypes that are currently at test are presented in more detail in Appendix B.

4 Measurements

4.1 Image acquisition

To measure the position of the grains at every moment, each grain received a painting pattern supposed to be followed using a Phantom v2512 high-speed camera. The camera we used can capture up to 500 000 images per second in a 1280×32 pixels grid. The light sources, two 100 W DC LEDs, were chosen for their high brightness and minimal fluctuation.

To follow this movement and be able to detect a rupture propagation, we had access to software specifically designed by a research engineer, allowing us to track every grain and plot their position at each frame, using image recognition on the paint pattern, shown in Figure 10. The pattern was recognized most of the time, and followed with varying accuracy, as detailed in Section 5.3.

A second measure, that of bulk deformation in the blocks, was made possible using Digital Image Correlation (DIC) using the software Ncorr [20, 21] and a slow speed camera at a low frame rate (1 image per second). It was used to measure the constraints applied to the different parts of the block. More details on the software used can be found in Appendix A.

4.2 Force measurement

The normal and shear forces are measured using force censors embedded in the frame. The measurement is ensured by a joint acquisition of force signals at 1 kHz and of the trigger signal (Section 4.4). The relatively fast acquisition allows for averages on the signal, reducing noise and increasing readability.

This measurement is mainly used to check that stick-slip occurs durring an experiment and to determine the friction coefficient. The expected force curve being the same as shown in Section 2.2, when the measured one is too different, the event can be ruled out. An example of such an event would be a small-scale rearrangement of the grains, in a localized part of the interface, leading neither to a normal force drop nor a propagative crack.

[2] At first glance, decreasing the thickness of the layer appears to be leading to a higher shear force threshold before rupture.

4.3 Photodiode signals

We use laser diodes coupled to photodiodes to detect propagating ruptures along the interface at the onset of sliding. This method consists in detecting the local displacement of the solid block when a rupture propagates. We put paint on the side of the blocks in a randomized pattern (spraying dark paint droplets) of characteristic width δ_P, the same as for the DIC measure. We then focused the beam of two lasers pointers directly on the painted surface using microscope objectives, in a dot of width δ_L. The blocks being transparent, except for the painting pattern, we then used convex lenses to focus back the laser beam on two photodiodes of response time τ_D on the other side of the experiment (Fig. 11).

To be able to detect a movement of length δ, we must have $\delta_P \gtrsim \delta$, of the same order to be sure to see a variation in brightness, but greater to avoid averaging effects, and $\delta_L \gtrsim \delta_P$, greater to be sure to see a variation in brightness, but of the same order to avoid averaging effects (Fig. 11). On a similar note, τ_D has to be far smaller than τ. In practice we had $\tau_D = 20\,\mathrm{ns}$, $\delta_L \simeq 100\,\mu\mathrm{m}$ and $\delta_P \simeq 10\,\mu\mathrm{m}$.

This method allows us to detect the rupture propagation front, but because of the randomization of the pattern, it cannot be calibrated to be used as a measurement of the displacement of the interface.

The model of photodiodes we used is the Thorlabs DET10A2. Their response time is given to be 1 ns in the case of a $50\,\Omega$ resistance, and their captor size is $0.8\,\mathrm{mm}^2$. we chose a very low response time to be as accurate as possible on the propagation speed detection, and a very small captor size, to allow maximum response to a converged laser beam.

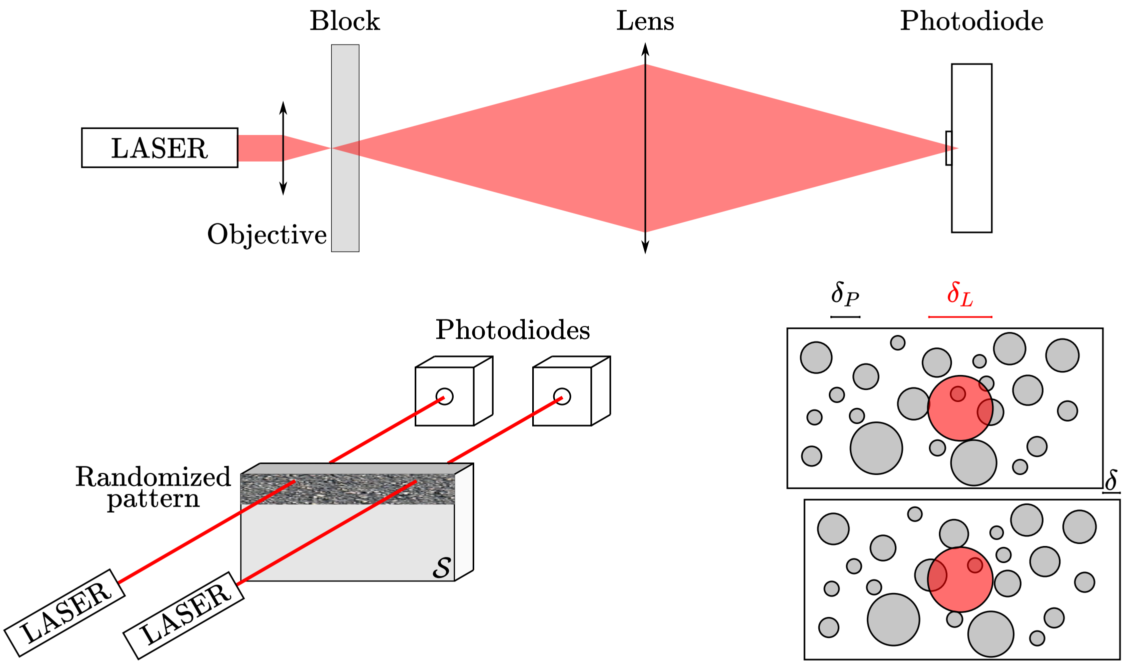

Figure 11: The photodiodes rupture speed measurent technique. **Top:** The laser is focused on the surface of the block covered with paint. It is then focused again on a high-speed photodiode. **Bottom left:** Schematic representation of the global setup. **Bottom right:** Comparison of the sizes of the δ. The condition $\delta_L \gtrsim \delta_P \gtrsim \delta$ is respected. The experimental values chosen where $\delta_L \simeq 100\,\mu\mathrm{m}$ and $\delta_P \simeq 10\,\mu\mathrm{m}$.

4.4 Trigger acquisition

Every rupture event is paired with wave propagation in the blocks. These waves can be detected using a sensitive enough accelerometer. We therefore paired the high-speed camera, the force acquisition, and the photodiodes signal acquisition to an accelerometer trigger. The basic principle of this trigger si to compare the accelerometer signal to a reference tension using a comparator, and to use the output as a triggering signal for all acquisitions. In addition to that, we paired the trigger to a pulse lengthener to light up a LED that allowed us to select the images of interest in the slow-speed acquisition camera record.

5 Results and discussion

5.1 Characterization of the system loading

5.1.1 Force measurements

We first need to characterize the loading of the interface and to detail the reaction to the forces applied to the system. When loading a coarse interface, the system goes regularly through a succession of stick and slip phases, as expected (Fig. 12).

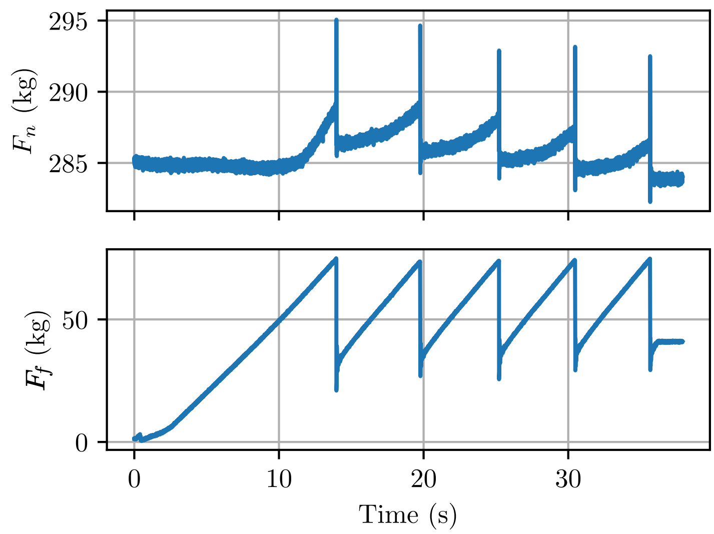

Figure 12: The stick-slip behavior in PMMA blocks. This series of events was obtained during a $50\,\mu\mathrm{m\,s^{-1}}$ translation. The fraction F_f/F_n at the rupture events gives a static friction coefficient $\mu_s \sim 0.26 \pm 0.02$. The spikes in the F_n curve correspond to a geometric effect due to the relative flexibility of the frame.

When adding grains at the interface, the stick-slip behavior remains. The shape of the shear force curve is typical of a stick-slip motion, even though its regularity is nothing like the one observed without grains (Fig. 13).

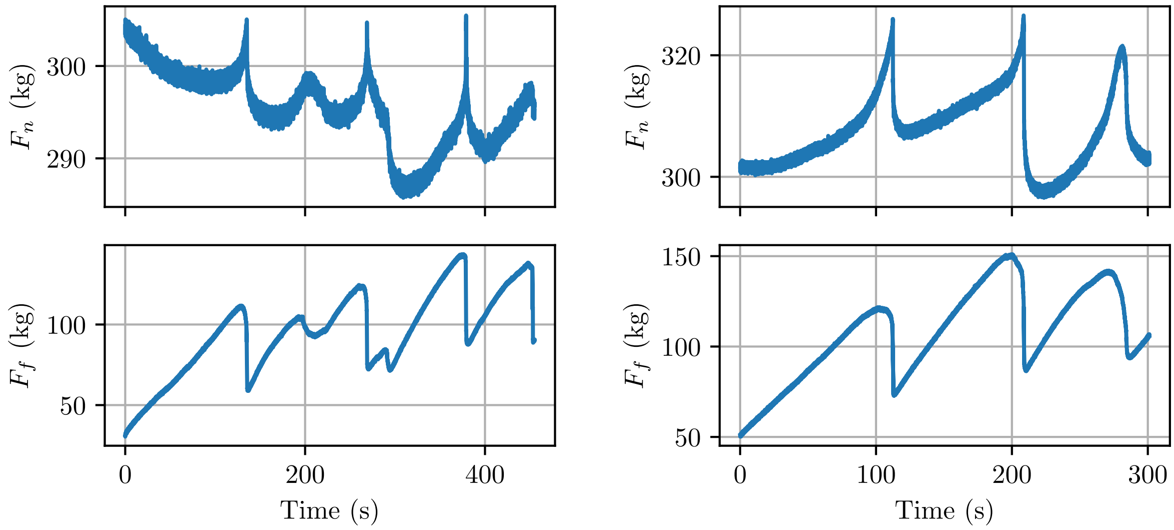

Figure 13: Two examples of force curves during granular stick-slip events. This series of events was obtained during a $10\,\mu\mathrm{m\,s}^{-1}$ translation. **Left:** With 5 mobile layers of grains (~ 5 mm). **Right:** With 3 mobile layers of grains (~ 3 mm).

Despite this irregularity, one can determine an equivalent μ_s for the interface. To do so, we measured F_n and F_f at the initiation of every slip event in the case of 3 mobile layers of grains (Fig. 14). This estimation of μ_s gives an idea of the maximum normal force we can apply to the system before reaching the limits in F_f of the motor. This quick study should be repeatable for different sizes of grains and different thicknesses of interface, which is an interesting prospect for the thesis that should follow this internship.

From Figure 14, we see that μ_s is not a characteristic of the interface, even for coarse interfaces as pointed out by previous studies [22].

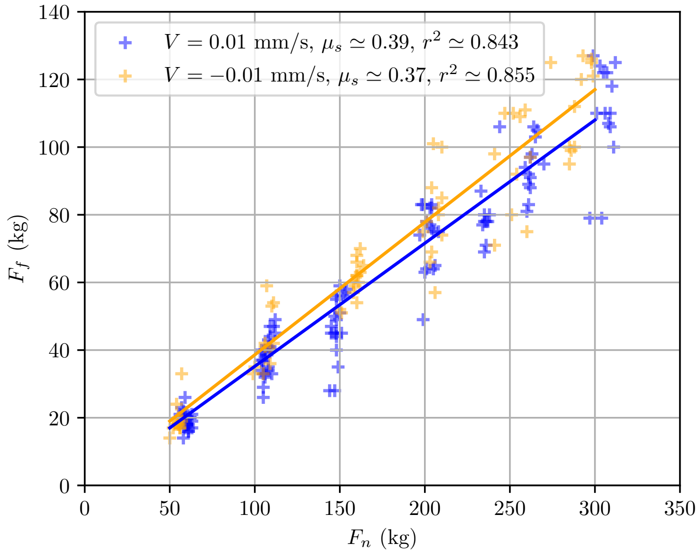

Figure 14: Shear force F_f at the initiation of a sliding event as a function of the normal force. The frictional interface is composed of 3 layers of mobile grains. The regression has a free origin because the force detector may have a constant shift. The orange data is obtained using a negative speed (in one direction) while the blue one is in the reverse direction. As a result, $\mu_s \simeq 0.38 \pm 0.05$ seems to be a good estimate of the static friction coefficient in that system.

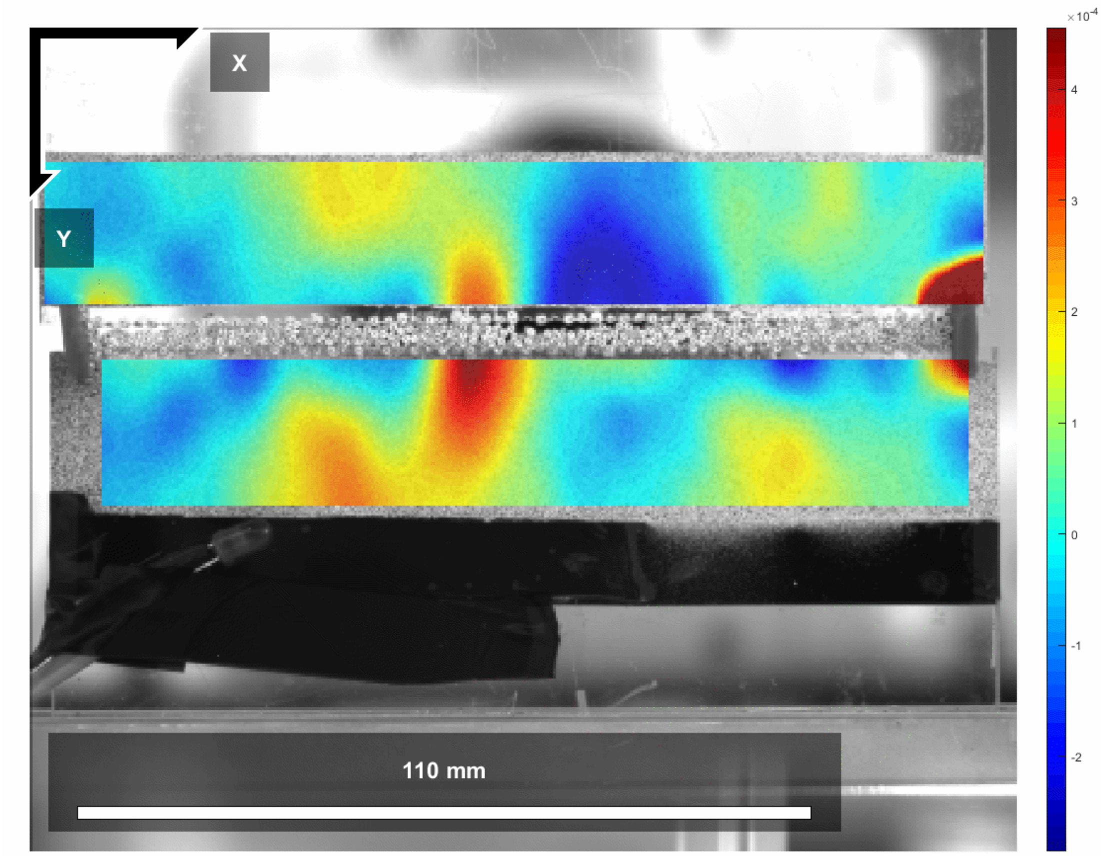

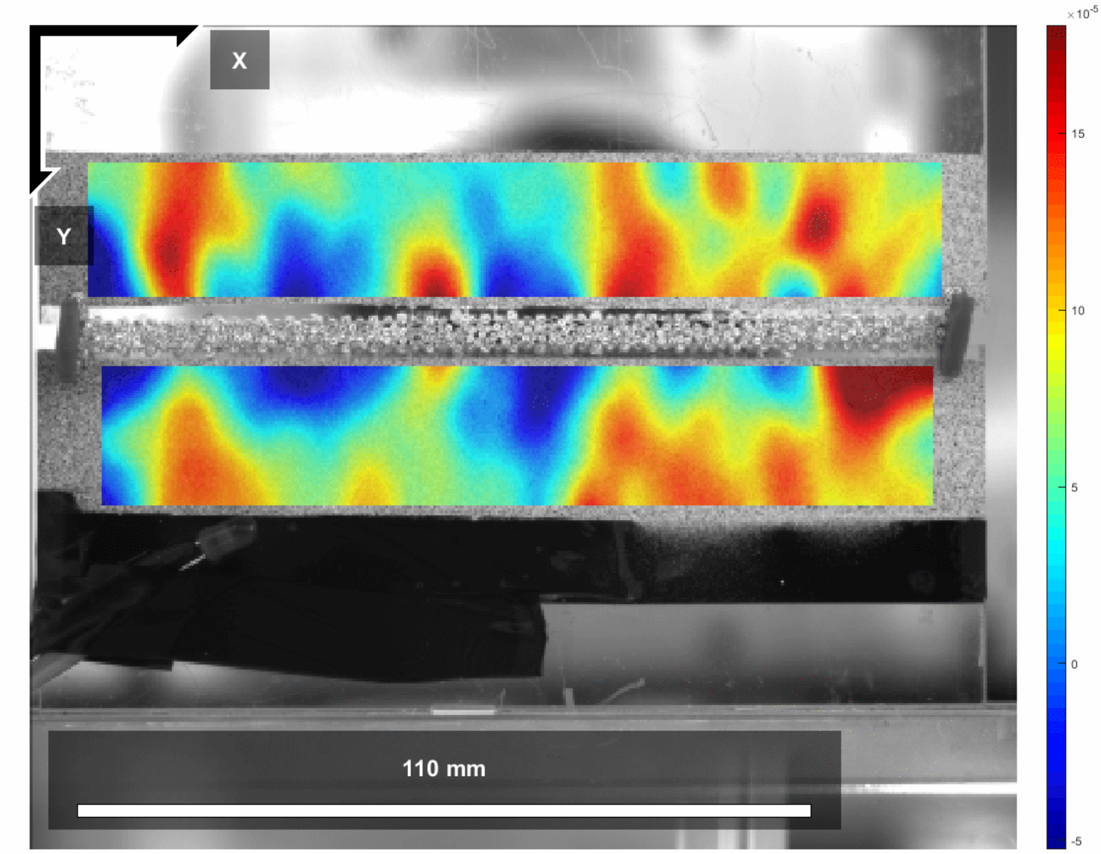

Figure 15: The output of the DIC software. It is a color map that associates a color to the strain level at each point of the interface. Both images are the y-y strains measures after a simple 300 kg normal compression. **Top:** An inhomogeneous repartition of constraints due to a misposition of the grains. **Bottom:** Improvement made to the first case, thanks to the deformation and strains characterization. The strains are four times smaller. *The color bars scales are different.*

5.1.2 Digital Image Correlation

Using the Digital Image Correlation (DIC) algorithm, we were able to measure the deformations of the bulk first during the normal load of the interface, allowing us to detect load irregularity. To obtain the deformation and the constraints applied to a block, we painted it with a randomized pattern, shown in Figure 10, and used Digital Image Correlation (DIC) [20] using the slow speed camera images.

Such a result allowed us to flatten the interface as much as possible, leading to a more homogeneous constraints repartition (Fig. 15). However, this method was of no use in the determination of the dynamics of the crack, due to the need for large scale images and therefore a low frame rate camera.

5.2 Propagating ruptures

5.2.1 Coarse interfaces

As explained in Section 4.3, the photodiodes can be used to determine the propagation speed of a rupture along an interface (Fig. 16). To be able to directly measure the speed of the rupture, the nucleation point must not be between the two laser beams, as in this case, the rupture would propagate simultaneously in both directions and be detected as faster than it really is. To control the location of the rupture, we used a stopper on the blocks. The principle of a stopper is to forbid movement on a corner of one block, accumulating the stress on that corner, and forcing the nucleation event to happen on that corner.

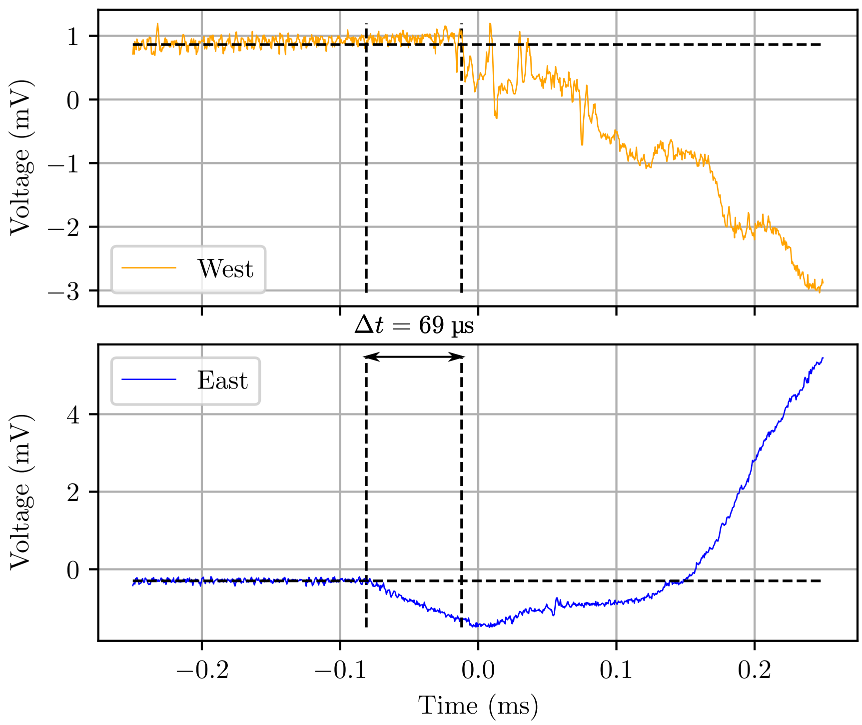

Figure 16: Photodiodes signal when transitioning from a stick phase to a slip phase in a coarse interface. This signal is high-passed, such that only rapid variations corresponding to large accelerations are detected. The crack speed is obtained by measuring the distance Δx between the two laser dots and dividing it by the time difference Δt between the two photodiodes signal changes.

By triggering the acquisition using an accelerometer in direct contact with the blocks, we obtained the speed of the ruptures. For the specific experiment shown in Figure 16, $C_f \simeq 1200\,\mathrm{m\,s^{-1}}$, which is an acceptable speed for a crack as it is below the Rayleigh wave speed $C_R = 1250\,\mathrm{m\,s^{-1}}$. This result is perfectly adequate with the literature [12, 13, 23].

5.2.2 Granular interface

We apply the same method in the case of a granular interface. A typical resulting photodiode signal is shown in Figure 17.

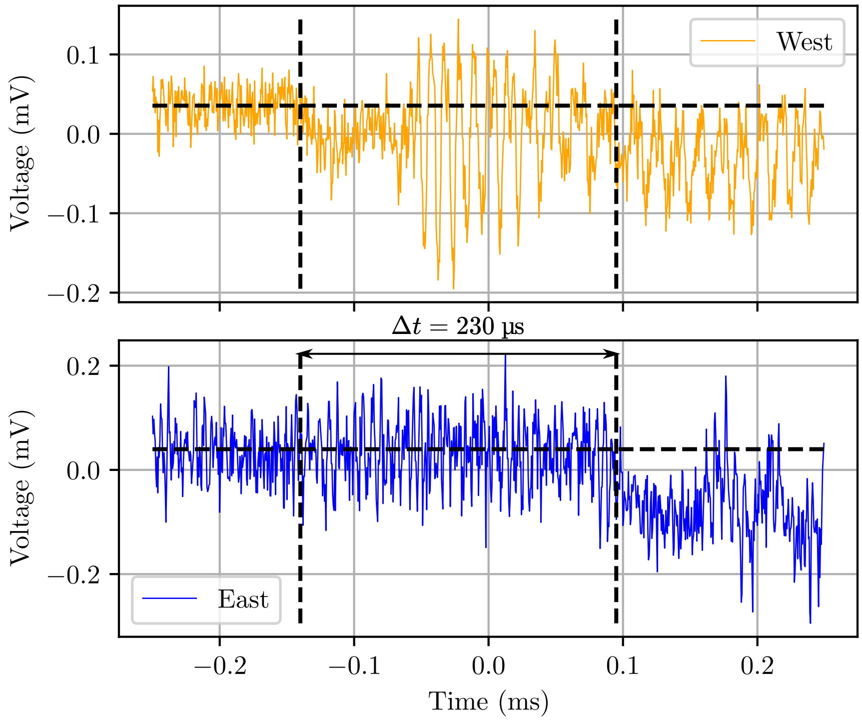

Figure 17: A typical output for the speed measure using the photodiodes in the granular case. The movements induced tend to be slower and smaller, and therefore less noticeable due to the high-pass filter applied to the photodiodes signals. On this particular sample, $\Delta t \simeq 230\,\mathrm{\mu s}$, $\Delta x = 8\,\mathrm{cm}$, $C \simeq 350\,\mathrm{m\,s^{-1}}$

In some cases, we measured high values of the rupture speed, higher than the dilatational wavespeed of the material. We recall that the dilatational wave speed is the maximal speed for information to travel in the material. These measurements of $C_f > C_d$ therefore correspond to experiments where the rupture nucleation occurs between the two photodiodes, instead of the corner of the interface, despite the stopper.

Taking that information into consideration, we started to only accept the cracks nucleating outside of the two laser beams. The speed of the average rupture then falls to systematically less than $1200\,\mathrm{m\,s^{-1}}$, usually around $800\,\mathrm{m\,s^{-1}}$. For the specific experiment shown in Figure 16, $C_f \simeq 300\,\mathrm{m\,s^{-1}}$, which is an acceptable speed for a crack as it is below the Rayleigh wave speed $C_R = 1250\,\mathrm{m\,s^{-1}}$.

5.3 Particle tracking

Using the high-speed camera, direct tracking of the grain expecting to see a rupture propagation could be possible. A very strong proof of the validity of a fracture propagation model would be to measure the displacement of the grains tethered to the blocks and to compare them to the prediction of fracture mechanics, shown to be valid for a non-granular interface (Section 2.4).

The time resolution allowed by the camera, $\tau_{cam} = 10^{-5}\,\mathrm{s}$, is better than the typical time of a crack event, which is at minimum $\tau_{crack} = L/C_R \simeq 15\,\mathrm{cm}/1250\,\mathrm{m\,s^{-1}} \sim 10^{-4}\,\mathrm{s}$, with L the length of the interface and C_R the Rayleigh wave speed. The camera reached 500 000 fps in a 1280x32 pixels grid.

As for the spatial resolution, the method we used to track the grain is to follow the grains templates shown in Figure 10 using software designed specifically for the task. The software uses Gaussian interpolation and convolutions to detect with a sub-pixel precision the position of every grain in a video. That resolution has to be better than the actual displacement of the grains, estimated to be of the order of δ_{LEFM}, defined in Section 2.4, to be able to measure said displacement.

To calibrate this position detection, we first measured the position of a fixed grain and measured the width of the optical noise (Fig. 18).

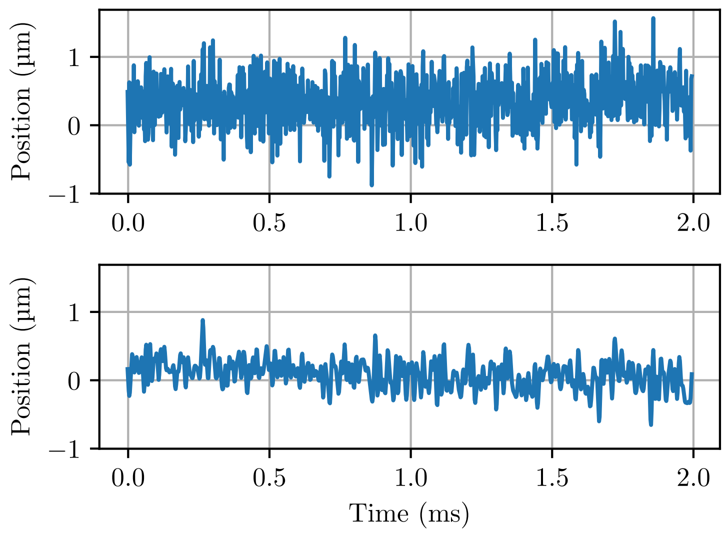

Figure 18: Calibration of the position measurement using the high-speed camera on the whole 15 cm interface ($10\,\mathrm{px\,mm^{-1}}$). **Top:** Position of a single grain, as measured by the camera while it is fixed. The constant noise is 0.04 pixel wide, *i.e.* 4 µm. **Bottom:** The same position after adequate signal processing, the noise falls down to 2 µm.

In Section 2.4, we have estimated the displacement of a bulk volume element associated with the propagation of a mode II crack. This calibration shows that the noise is too wide for the position of the grains to be accurately measured all along the interface during a rupture event, as the expected movement order is $\delta_{LEFM} = 1\,\mu\mathrm{m}$. To tackle that issue, we decided to reduce the filmed width by zooming on a part of the interface, expecting the noise to be the same in pixels, but smaller in reality. The result is shown in Figure 19.

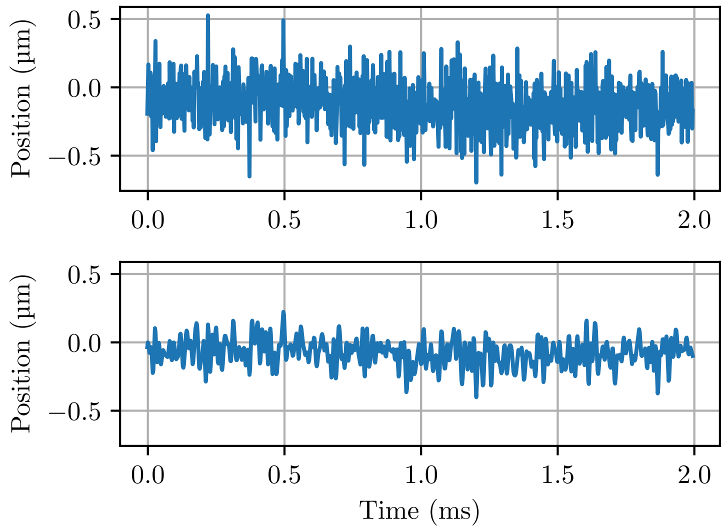

Figure 19: Calibration of the position measurement when zooming on 5 cm of the interface ($30\,\mathrm{px\,mm^{-1}}$). **Top:** Position of a single grain, as measured by the camera while it is fixed. The constant noise is 1 µm wide. **Bottom:** The same position after adequate signal processing, the noise falls down to 0.5 µm.

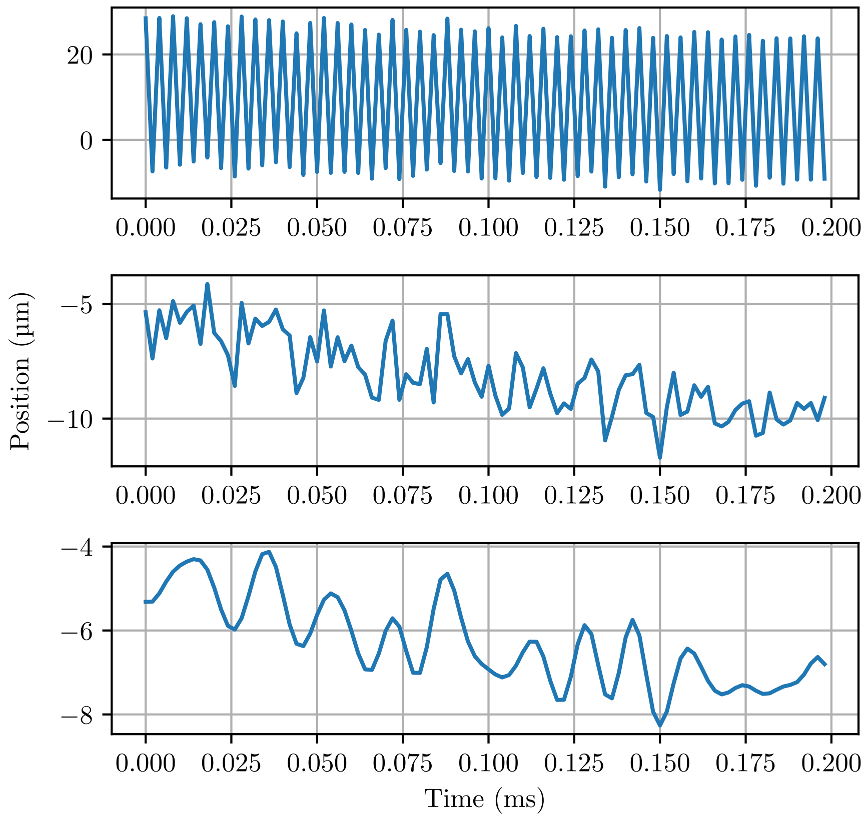

Figure 20: The sub-pixel position correction process. **Top:** The unfiltered position tracking outcome, oscillating between two positions because of the binning of the camera. **Middle:** The position after removing the oscillation. **Bottom:** The position after applying a high pass filter and removing as much noise as possible. The tracking method used is inherently prone to some form of noise. This noise is relatively white, and therefore very hard to clean, and is of the same order of magnitude as the crack propagation induced movement we expect from this system.

The noise rate is then smaller but of the same order as δ_{LEFM}, which would make the movement very hard to isolate from the noise. On top of that, we expect the grains to make the displacement even smaller. The spatial resolution is therefore the real problem of this method, as the tracking is not foolproof and has a large standard deviation noise. Figure 20 shows a typical movement curve we see in a rupture event, and details the different filtering passes applied to the data.

5.4 Discussion

These results better characterize the rupture phenomenon of a granular frictional interface at the onset of sliding. First, the photodiodes measurement allowed us to determine the velocity and time scale for the rupture propagation, imposing a time resolution for further experiments. This time scale being $\tau_{crack} = 10^{-4}$ s, it conditioned the usage of a high-speed camera for any direct optical observation of the crack propagation.

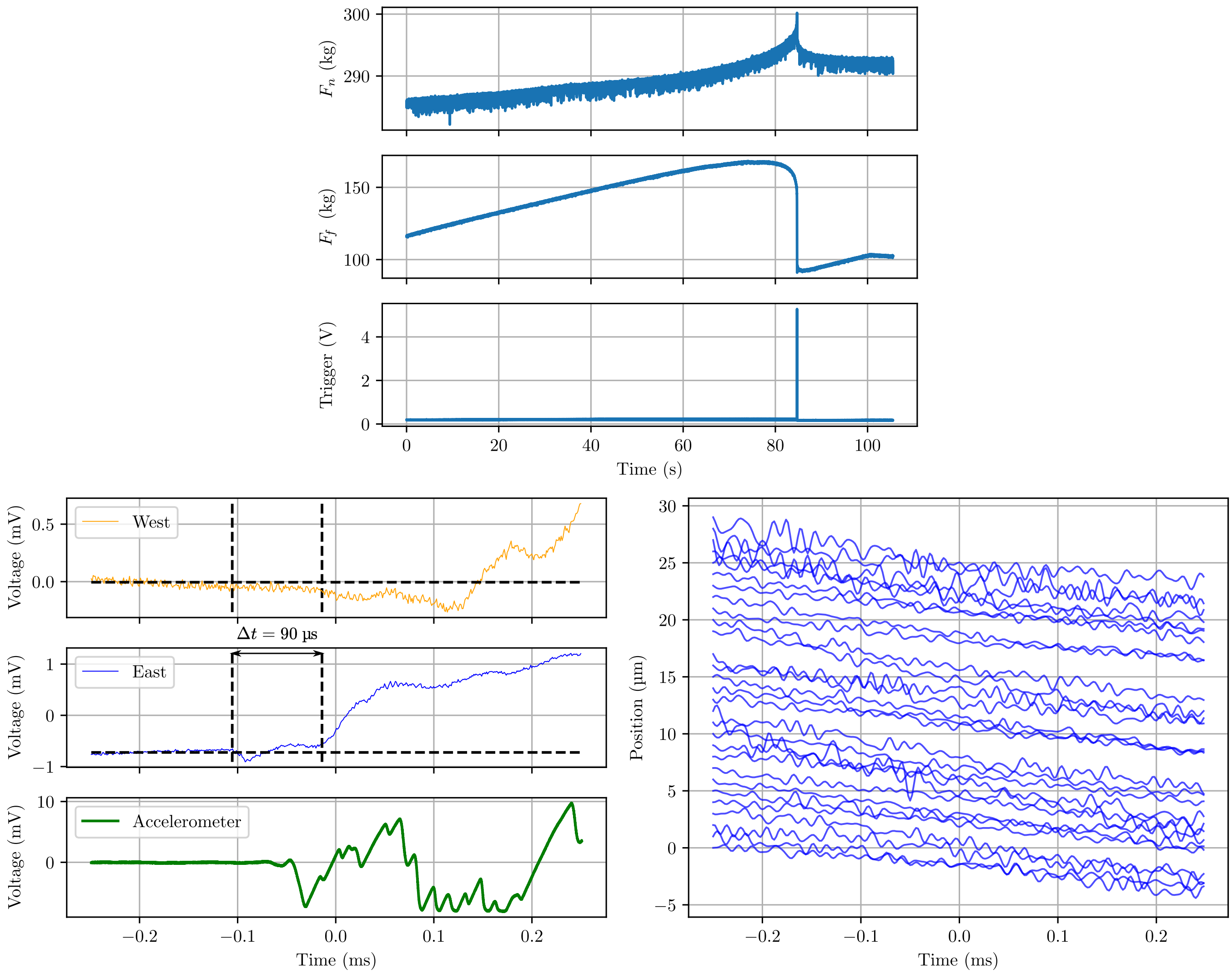

Figure 21: All the measurements available for a single event. **Top:** The forces measurement, and the trigger signal created to launch the other two acquisitions. **Left:** The photodiodes signals and the accelerometer signal. For this event, $C_f \simeq 880\,\mathrm{m\,s^{-1}}$. **Right:** The positions of the tracked grains tracked using he high-speed camera on 10 cm of the interface ($18\,\mathrm{px\,mm^{-1}}$). The initial position of each grain is shifted proportionally to its real position on the interface.

The determination of the spatial scale was possible thanks to the Linear Elastic Fracture Mechanics solutions applied to frictional interfaces. It gave us a scale, $\delta_{LEFM} = 1\,\mu\mathrm{m}$, to compare to our camera resolution. This comparison reveals a mismatch between the camera resolution and the expected amplitude of the displacement, which prevents us from having direct optical access to the crack propagation.

To gain this access, two options are available. The first one is to follow the non-granular frictional crack propagation literature [15] and implement a new measurement based on an array of strain gauges. These strain gauges are electronic components of which the resistance varies with their deformation, along with that of the block they are onto. Acquiring the strain gauges signal at high frequency should allow us to follow the rupture propagation by detecting the variations of the strain field at each measurement point. The second option would be to increase the displacement (or to slow down the rupture and choose a better-resolved camera), which in practice means reducing the stiffness of the blocks. A third option would be to change the properties of the grains, but the effects of such a change are unknown.

6 Conclusion

As conclusion, the main result of this internship is the detection of a propagating rupture and the characterization of its speed and displacement scale. The optical tracking method we used gave no significant result, in agreement with the theoretical expectation in a perturbative approach of the granular interface.

To tackle this resolution issue, and to compare our system to the brittle fracture theory presented in Section 2.4, we plan to use an array of strain gauges all along the interface. This should allow for much more precision in the measurement of the displacements associated with the crack tip propagation. Slowing the crack down by using different blocks or grains could also be included in future work.

Finally, we plan a better characterization of the impact of both the nature and the thickness of the granular material, especially on the properties of the cracks and their propagation.

References

[1] J. Byerlee. “The mechanics of stick-slip”. In: *Tectonophysics* 9.5 (1970), pp. 475–486. ISSN: 0040-1951.

[2] W. F. Brace and J. D. Byerlee. “Stick-Slip as a Mechanism for Earthquakes”. In: *Science* 153.3739 (1966), pp. 990–992. ISSN: 0036-8075.

[3] A. Cochard and R. Madariaga. “Dynamic faulting under rate-dependent friction”. In: *pure and applied geophysics* 142.3 (1994), pp. 419–445.

[4] J. Trømborg et al. “Transition from Static to Kinetic Friction: Insights from a 2D Model”. In: *Phys. Rev. Lett.* 107 (7 2011), p. 074301.

[5] C. Marone. “LABORATORY-DERIVED FRICTION LAWS AND THEIR APPLICATION TO SEISMIC FAULTING”. In: *Annual Review of Earth and Planetary Sciences* 26.1 (1998), pp. 643–696.

[6] A. J. Weymouth et al. “Atomic Structure Affects the Directional Dependence of Friction”. In: *Phys. Rev. Lett.* 111 (12 2013), p. 126103.

[7] C. M. Mate. *Tribology on the Small Scale: A Bottom Up Approach to Friction, Lubrication, and Wear*. eng. Vol. 6. Mesoscopic Physics and Nanotechnology. Oxford: Oxford University Press, 2007. ISBN: 0198526784.

[8] C. A. Coulomb. *Théorie des machines simples en ayant égard au frottement de leurs parties et à la roideur des cordages*. Bachelier, 1821.

[9] F. P. Bowden, F. P. Bowden, and D. Tabor. *The friction and lubrication of solids*. Vol. 1. Oxford university press, 2001.

[10] F. P. Bowden and D. Tabor. “The Friction and Lubrication of Solids”. In: *American Journal of Physics* 19.7 (1951), pp. 428–429.

[11] T. Baumberger and C. Caroli. “Solid friction from stick–slip down to pinning and aging”. In: *Advances in Physics* 55.3-4 (2006), pp. 279–348.

[12] S. Rubinstein, G Cohen, and J Fineberg. “Dynamics of precursors to frictional sliding”. In: *Physical review letters* 98.22 (2007), p. 226103.

[13] K. Xia, A. J. Rosakis, and H. Kanamori. “Laboratory Earthquakes: The Sub-Rayleigh-to-Supershear Rupture Transition”. In: *Science* 303.5665 (2004), pp. 1859–1861. ISSN: 0036-8075.

[14] S Latour et al. “Characterization of nucleation during laboratory earthquakes”. In: *Geophysical Research Letters* 40.19 (2013), pp. 5064–5069.

[15] I. Svetlizky, E. Bayart, and J. Fineberg. “Brittle fracture theory describes the onset of frictional motion”. In: *Annual Review of Condensed Matter Physics* 10 (2019), pp. 253–273.

[16] L. B. Freund. *Dynamic fracture mechanics*. Cambridge university press, 1998.

[17] N. Lapusta and J. R. Rice. “Nucleation and early seismic propagation of small and large events in a crustal earthquake model”. In: *Journal of Geophysical Research: Solid Earth* 108.B4 (2003).

[18] D. A. Geller et al. “Stick-slip behavior in a continuum-granular experiment”. In: *Phys. Rev. E* 92 (6 2015), p. 060201.

[19] L. Buijze et al. “Nucleation of Stick-Slip Instability Within a Large-Scale Experimental Fault: Effects of Stress Heterogeneities Due to Loading and Gouge Layer Compaction”. In: *Journal of Geophysical Research: Solid Earth* 125.8 (2020), e2019JB018429.

[20] T. Chu, W. Ranson, and M. A. Sutton. “Applications of digital-image-correlation techniques to experimental mechanics”. In: *Experimental mechanics* 25.3 (1985), pp. 232–244.

[21] J Blaber, B Adair, and A Antoniou. “Ncorr: open-source 2D digital image correlation matlab software”. In: *Experimental Mechanics* 55.6 (2015), pp. 1105–1122.

[22] O. Ben-David and J. Fineberg. “Static friction coefficient is not a material constant”. In: *Physical review letters* 106.25 (2011), p. 254301.

[23] S. M. Rubinstein, G. Cohen, and J. Fineberg. “Detachment fronts and the onset of dynamic friction”. In: *Nature* 430 (2004), pp. 1005–1009.

Appendix

A DIC

The DIC software we use was an older version of Ncorr [21], an Open-Source 2D Digital Image Correlation Matlab Software. As I am not an expert in DIC and am not familiar with the parameters of the Ncorr software, I decided to mainly use the defaults parameters, whenever possible.

Some problems emerged from the usage of the software. First, the area to which we apply the DIC algorithm must always be contained strictly within the random pattern, at the risk of polluting nearby parts of the image (22). Second, the resolution we achieved using Ncorr was not enough to properly detect changes as little as the nucleation of a crack, although this could be due only to my inability to properly use the software. Finally, the time needed by the algorithm to complete, even on small areas, was of the order of 5 minutes for each image considered, and therefore non-acceptable for large-scale data analysis.

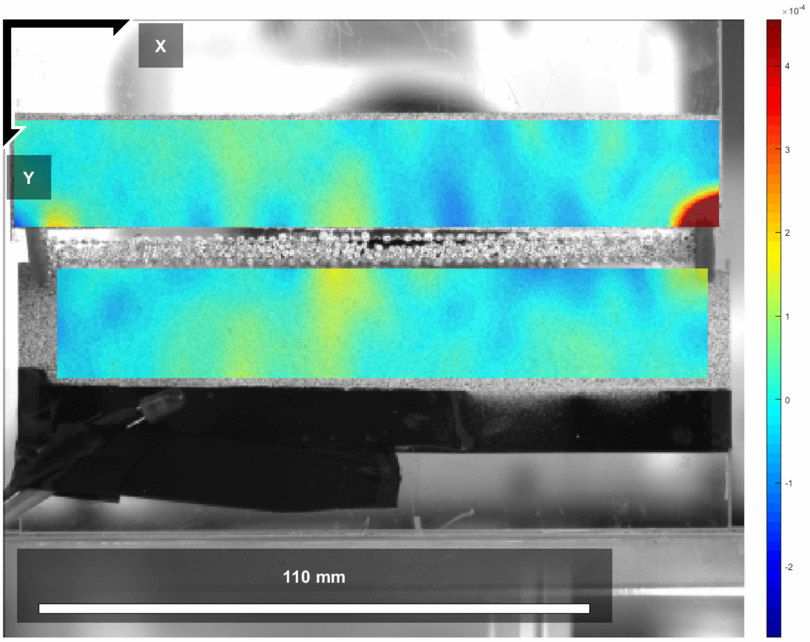

Figure 22: When taking into the DIC area a part of the image that has no easy to track pattern on it, the results are distorted. For example, the bottom right corner of the top block here appears as the only strained zone, while actually, this is the result of a tracking issue.

B Blocks design

The detailed design of the block is still one of the major issues of this work. Among the various possibilities, here is a list of the main parameters:

- Size of the grain
- Depth of the grain slot
- thickness of the block
- types of grains
- grains position along the interface

- shape of the interface

In Figure 23 and Figure 24 are described the main type of blocks we used, as well as a prototype that is yet to be tested.

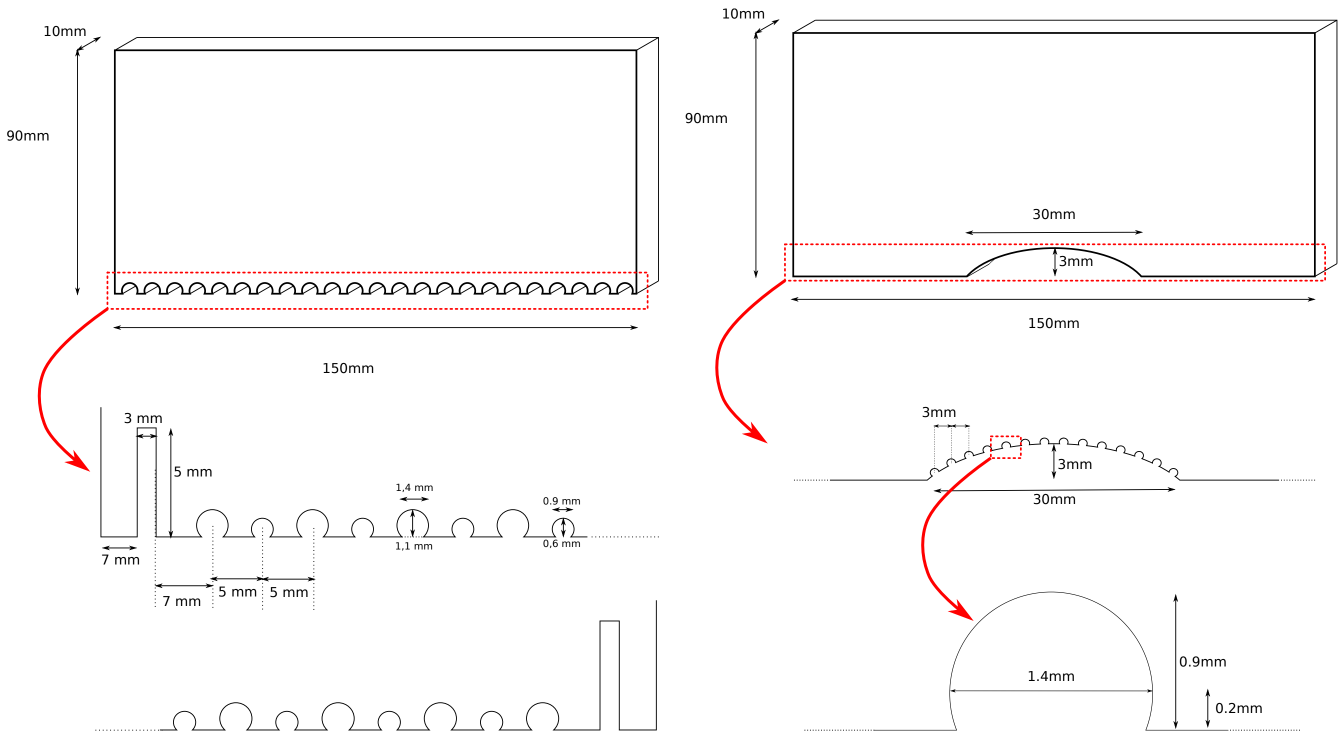

Figure 23: The left block is the standard type of blocks we used. Its main feature is the alternating pattern of small and large grains, avoiding crystallization effects. The right block is a prototype that should be tested next month, with hope to trigger to nucleation outside of the granular interface, and to measure its propagation across the interface.

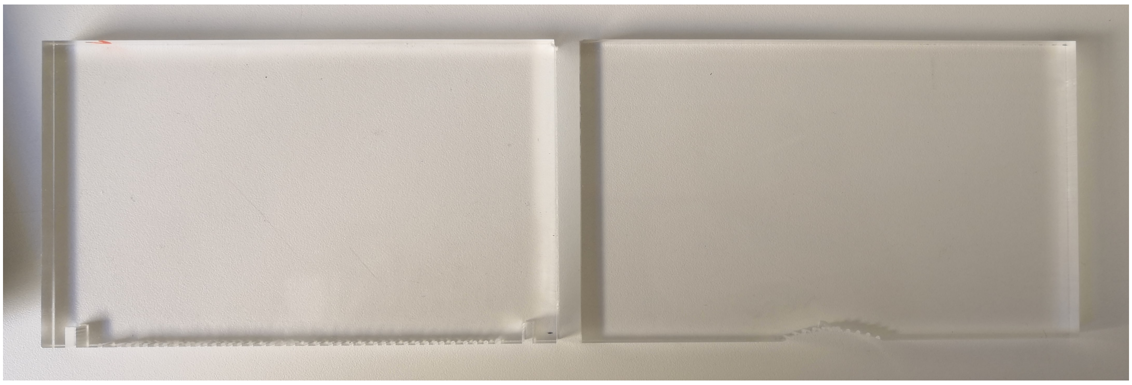

Figure 24: Photo of the blocks described in the previous Figure.